International Journal of Applied Information Systems (IJAIS) ISSN : 2249-0868
Foundation of Computer Science FCS, New York, USA
Volume 12 - No. 29, May 2020 - www.ijais.org

Multiselectivity Spatio-Temporal Analysis for Motion and Velocity Capture

Mohamed EL Aallaoui
Department of Statistics and Applied Mathematics in Economics
FSJES Aïn Sebaâ, Hassan II University, Casablanca Morocco

ABSTRACT

This paper focuses on the development of a new 2D time wavelets family for image sequence that can capture different motion in image sequence, ranging from highly directional ones to fully isotropic ones. We propose a multiselectivity spatio-temporal analysis, defined by isotropic and multidirectional decomposition with different angular selectivity. The result is a dictionary of wavelet transform with different selectivity level, which provides a theoretical tool to select a best representation for motion and velocity. This representation was used to developer a velocity capture algorithm in image sequence. The Experimental results demonstrate the effectiveness of the proposed approach.

Keywords

2D+time wavelets, Velocity capture, Motion analysis, Multiselectivity analysis, Angular selectivity

1. INTRODUCTION

Motion and velocity estimation is typically the most compute intensive part of video processing, it has become of great interest in several areas of video analysis such as motion compensated image coding [1, 2], civil and military applications of object tracking and autonomous navigation[3, 4], identification of anomalies using image processing in biological and medical images[5], spatiotemporal video segmentation [6, 7, 8], obstacle evasion in mobile robotic [4, 9], sport training, comparing behaviors respect a mathematical model [10, 11],...
Motion estimation is an ill-posed problem as the motion is in three dimensions but the images are a projection of the 3D scene onto a 2D plane [12], numerous techniques have been proposed to tackle such an inverse problem. Four methods are mainly used in motion and velocity estimation [13, 14]. Those are: 1) Block matching; 2) Multiresolution filtering (with or without compensation); 3) Optical flow; 4) Non-transmission of movement information.
So far most algorithms for three-dimensional motion estimation use optical flow. Optical flow approachs are based on the assumption that pixel-values between frames change only because of motion, but not on regions or objects. They assume that the object is constant from frame to frame and that the object signature does not deform over time. They are not inherently scalable either. These approaches generally cannot appropriately handle scenarios including noise, time varying object signatures, and temporary ocelusions because the temporal support over which they operate is too limited, this limitation can be relaxed by the extensions of continuous wavelet transform to spatio-temporal space, these spatio-temporal wavelet Transforms (2D+T WT) provide a good motion estimation in image sequences[15, 16, 17, 18], and give an efficient alternative framework to the optical flow. Extensions of continuous wavelet transform to multiple dimensions have been successfully used for the analysis and classification of 2D+time signals [13]. The group of 2D analysis parameters, i.e., usually position, scale and rotation, has been extended to speed, acceleration and deformation. This has led to various types of time dependent wavelets. We may cite for instance, 2D+T Morlet wavelet [15, 16], 2D+T Gaussian-Conical-Morlet (GCM) wavelet [17], Galilei wavelets[18, 13], Accelerated spatio-temporal wavelet [19]...
Real image sequence contain very different motions, ranging from very oriented ones, like translations, to more isotropic motions, like rotation motions. Between these two extreme behaviors, we find, for instance, curvilinear motions [13, 14]. Each speed of these motions is well represented by 2D+time wavelets with different angular selectivity. However, in all the spatio-temporal wavelet transforms mentioned above, the wavelets share the same angular selectivity. In order to overcome this limitation of velocity capture, we construct a new spatio-temporal wavelets with different angular selectivity, the construction of these wavelets is done separately in frequency space, by a spatial filter and a temporal 1D filter. We obtain a multiselectivity spatio-temporal analysis which can capture the different structures of motion and velocity.
The outline of the paper is as follows. In section 2, we recall the basic formulas of 2-D continuous wavelet transform. These formulas will be extended to the 2D+T case in section 3. In section 4 we propose a multiselectivity spatio-temporal analysis defined by a new spatio-temporal wavelets with different angular selectivity. The design and implementation problems and how to use this analysis to capture velocity and analyze motion, are discussed in section 5 and 6. We report the results of our experiments in section 7 and conclude the paper in section 8.

2. PRELIMINARIES: 2-D CONTINUOUS WAVELET TRANSFORM

In order to fix the notations, we first recall the basic formulas of 2-D continuous wavelet transform. Let $f \in L^2(\mathbb{R}^2)$ be an image of finite energy. Given a wavelet $\psi \in L^2(\mathbb{R}^2)$ satisfying the admissibility condition

$$c_\psi = 2\pi^3 \int_{\mathbb{R}^2} \frac{|\widehat{\psi}^*(\vec{k})|^2}{|\vec{k}|^2},\ d\vec{k} < +\infty. \tag{1}$$

The hat denotes the standard Fourier transform on $L^2(\mathbb{R}^2)$, these condition is called the wavelet admissibility condition [20, 21]. To guarantee that this integral is finite, we must ensure that $\widehat{\psi}(\vec{0}) = 0$, which explains why wavelets must have a zero average. This condition is nearly sufficient. If $\widehat{\psi}(\vec{0}) = 0$ and $\widehat{\psi}$ is continuously differentiable, then the admissibility condition is satisfied.
The continuous wavelet transform of f is the function[20, 22]

$$W_{\vec{b},a,\theta} = \langle \psi_{\vec{b},a,\theta} | f \rangle \tag{2}$$

$$= a^{-2} \int_{\mathbb{R}^2} \psi^*\big(r_\theta^{-1} \frac{\vec{x} - \vec{b}}{a}\big)\, f(\vec{x})\, d^2\vec{x} \tag{3}$$

$$= a^2 \int_{\mathbb{R}^2} \widehat{\psi}^*(a r_\theta^{-1} \vec{k})\, \widehat{f}(\vec{k})\, e^{i\vec{k}\cdot\vec{b}}\, d^2\vec{k}, \tag{4}$$

where the wavelet $\psi_{\vec{b},a,\theta}$ is an L^1-normalized copy of ψ, translated by $\vec{b} \in \mathbb{R}^2$, dilated by $a \in \mathbb{R}^*_+$ and rotated by $\theta \in S_1 \simeq [0, 2\pi)$.

$$r_\theta^{-1} \begin{pmatrix} cos\,\theta & sin\,\theta \\ -sin\,\theta & cos\,\theta \end{pmatrix}. \quad (5)$$

These formulas will be extended to the 2D+T case in following section.

3. 2D+T CONTINUOUS WAVELET TRANSFORM

Image sequence is an object of three dimensions: spatial (2D) and temporal (1D), for analysis this sequence, we must first build a (2D+T) Hilbert spatio-temporal space, Correspondingly, we consider the space of square-integrable signals over space and time $\mathcal{H} = L^2(\mathbb{R}^2 \times \mathbb{R}, d\vec{x}dt)$. The corresponding scalar product and norm are

$$\langle g|f\rangle = \int_{\mathbb{R}}\int_{\mathbb{R}^2} g^*(\vec{x},t)\, f(\vec{x},t)\, d\vec{x}dt \quad (6)$$

$$= \int_{\mathbb{R}}\int_{S_1}\int_{\mathbb{R}^+} g^*(\rho,\sigma,t)\, f(\rho,\sigma,t)\, d^2s dt, \quad (7)$$

and

$$\|f\|^2 = \int_{\mathbb{R}^2}\int_{\mathbb{R}} |f(\vec{x},t)|^2\, d\vec{x}dt \quad (8)$$

$$= \int_{\mathbb{R}}\int_{S_1}\int_{\mathbb{R}^+} |f(\rho,\sigma,t)|^2 d^2s dt, \quad (9)$$

where $\vec{x} = (\rho, \sigma)$, $\rho = \|\vec{x}\|$, $\sigma = \arg\vec{x}$ and $d^2s = \rho d\rho d\sigma$. The Fourier transform of f is defined, as usual, by

$$\widehat{f}(\vec{k},w) = (2\pi)^{-3/2}\int_{\mathbb{R}}\int_{\mathbb{R}^2} e^{-j(\vec{k}\vec{x}+wt)} f(\vec{x},t)\, d\vec{x}dt \quad (10)$$

$$= \frac{1}{(2\pi)^{3/2}}\int_{\mathbb{R}}\int_{S_1}\int_{\mathbb{R}^+} J(r,\theta,w,\rho,\sigma,t)\, d^2s dt, \quad (11)$$

where

$$J(r,\theta,w,\rho,\sigma,t) = e^{-j(r\rho cos(\sigma-\theta)+wt)} f(\rho,\sigma,t), \quad (12)$$

$\vec{k}$ is the spatial frequency,w is the temporal frequency, $\vec{k} = (r,\theta)$, $r = \|\vec{k}\|$ and $\theta = \arg\vec{k}$.
The relationship between the energy distribution of a static object $f(\vec{x},t) = h(\vec{x})$ and the energy of the same object in linear motion $f_{\vec{v}}(\vec{x} - \vec{v}t, t) = h(\vec{x} - \vec{v}t)$ can be mathematically represented by Fourier pairs. For a static object we have:

$$\begin{aligned}\widehat{f}(\vec{k},w) &= (2\pi)^{-3/2}\int_{\mathbb{R}}\int_{\mathbb{R}^2} e^{-j(\vec{k}\vec{x}+wt)} f(\vec{x},t)\, d\vec{x}dt \\ &= (2\pi)^{-3/2}\int_{\mathbb{R}}\int_{\mathbb{R}^2} e^{-j(\vec{k}\vec{x}+wt)} h(\vec{x})\, d\vec{x}dt \\ &= (2\pi)^{-3/2}\int_{\mathbb{R}^2} e^{-j(\vec{k}\vec{x})} h(\vec{x}) d\vec{x}\int_{\mathbb{R}} e^{-j(wt)}\, dt \\ &= \widehat{h}(\vec{k})\delta(w),\end{aligned}$$

and

$$\begin{aligned}\widehat{f_{\vec{v}}}(\vec{k},w) &= (2\pi)^{-3/2}\int_{\mathbb{R}}\int_{\mathbb{R}^2} e^{-j(\vec{k}\vec{x}+wt} f_{\vec{v}}(\vec{x},t)\, d\vec{x}dt \\ &= (2\pi)^{-3/2}\int_{\mathbb{R}}\int_{\mathbb{R}^2} e^{-j(\vec{k}\vec{x}+wt)} h(\vec{x}-\vec{v}t)\, d\vec{x}dt \\ &= (2\pi)^{-3/2}\int_{\mathbb{R}}\int_{\mathbb{R}^2} e^{-j(\vec{k}\vec{y})-j(\vec{k}\vec{v}+w)t} h(\vec{y})\, d\vec{y}dt \\ &= (2\pi)^{-3/2}\int_{\mathbb{R}^2} e^{-j(\vec{k}\vec{y})} h(\vec{y}) d\vec{y}\int_{\mathbb{R}} e^{-j(\vec{k}\vec{v}+w)t}\, dt \\ &= \widehat{h}(\vec{k})\delta(\vec{k}\vec{v}+w).\end{aligned}$$

The energy of static object is concentrated in the null frequencies plane, $w = 0$. In the presence of a linear motion, this energy is distributed over a plane defined by:

$$\vec{k}\vec{v} + w = 0. \quad (13)$$

Several motion operators can be applied to the mother wavelet ψ, namely, scaling (D^a), translation ($T^{\vec{b}}$), rotation (R^β) and speed tuning (A^c)[13, 14].

3.1 Scaling

$$[D^a\psi](\vec{x},t) = a^{-3/2}\psi(\frac{\vec{x}}{a},\frac{t}{a}) \quad (14)$$

or, equivalently in the space of Fourier transforms,

$$\widehat{[D^a\psi]}(\vec{k},w) = a^{3/2}\widehat{\psi}(a\vec{k},aw), \quad (15)$$

where $a \in \mathbb{R}^+$.

3.2 Space-time translation

$$[T^{\vec{b},\tau}\psi](\vec{x},t) = \psi(\vec{x}-\vec{b},t-\tau), \quad (16)$$

or, equivalently in the space of Fourier transforms,

$$\widehat{[T^{\vec{b},\tau}\psi]}(\vec{k},w) = e^{-j(\vec{k}.\vec{b}-w\tau)}\widehat{\psi}(\vec{k},w), \quad (17)$$

where $(\vec{b},\tau) \in \mathbb{R}^2 \times \mathbb{R}$.

3.3 Rotation

$$[R^\beta\psi](\vec{x},t) = \psi(r_\beta^{-1}\vec{x},t), \quad (18)$$

or, equivalently in the space of Fourier transforms,

$$\widehat{[R^\beta\psi]}(\vec{k},w) = \widehat{\psi}(r_\beta^{-1}\vec{k},w), \quad (19)$$

where

$$r_\beta^{-1} \begin{pmatrix} cos\,\beta & sin\,\beta \\ -sin\,\beta & cos\,\beta \end{pmatrix}. \quad (20)$$

And $\beta \in [0, 2\pi]$.

3.4 Speed tuning

The speed tuning transformation, denoted A^c, can be as two independent scaling operation performed on the spatial and temporel variables.

$$[A^c\psi](\vec{x},t) = \psi(c^{-p}\vec{x},c^q t), \quad (21)$$

where $c \in \mathbb{R}^+$ and $(p,q) \in \mathbb{R}^2$, the speed tuning transformation is unitary

$$\begin{aligned}\|\psi\|^2 &= \|[A^c\psi]\|^2 \\ &= \int_{\mathbb{R}}\int_{\mathbb{R}^2} |\psi(c^{-p}\vec{x},c^q t)|^2 d\vec{x}dt \\ &= c^{2p-q}\int_{\mathbb{R}}\int_{\mathbb{R}^2} |\psi(\vec{x},t)|^2 d\vec{x}dt \\ &= c^{2p-q}\|\psi\|^2\end{aligned}$$

Hence

$$q = 2p. \quad (22)$$

In the space of Fourier transforms,

$$\widehat{[A^c\psi]}(\vec{k},w) = \widehat{\psi}(c^p\vec{k},c^{-q}w), \quad (23)$$

the application the speed tuning transformation to $c\vec{v}$ plane of the equation 13 yields that

$$c^p\vec{k}\vec{v} = -c^{-q}w, \quad (24)$$

$$w = -c^{q+p}\vec{k}\vec{v} \quad (25)$$
$$w = -c\vec{k}\vec{v}, \quad (26)$$

this requires that

$$p + q = 1. \quad (27)$$

The system formed by the constraints 22 and 27 thus leads to the admissible values: $q = 2/3$ and $p = 1/3$.
These transformation operators written above have identified a parameter space Λ, which increases the capacity of the wavelet analysis beyond the traditional parameters of scale (frequency) and the position. The new parameter space is:

$$\Lambda = \{(a, \vec{b}, \tau, \beta, c) \in \mathbb{R}^+ \times \mathbb{R}^2 \times \mathbb{R} \times [0, 2\pi] \times \mathbb{R}^+\}. \quad (28)$$

The application of all operators leads to a transformation composite Ω_Λ consisting of: spatio-temporal dilation, spatial and temporal translation, rotation, and speed tuning. Its application to a 2D+t wavelet ψ gives:

$$\Omega_\Lambda\psi(\vec{x}, t) = T^{\vec{b},\tau}R^\beta A^c D^a\psi(\vec{x}, t), \quad (29)$$

and by replacing each operator by its expression of transformation, we obtain the developed expression of the 2D+t wavelet ψ,

$$[\Omega_\Lambda\psi](\vec{x}, t) = a^{-3/2}\psi\big(\frac{c^{-p}}{a}r_\beta^{-1}(\vec{x} - \vec{b}), \frac{c^q}{a}(t - \tau)\big). \quad (30)$$

In the same way, for the Fourier space:

$$\widehat{[\Omega_\Lambda\psi]}(\vec{k}, w) = a^{3/2}\psi\big(ac^p r_\beta^{-1}(\vec{k}), ac^{-q}w\big)e^{-j(\vec{k}.\vec{b}-w\tau)}. \quad (31)$$

If the wavelet ψ satisfies

$$c_\psi = 2\pi^3 \int_{\mathbb{R}}\int_{\mathbb{R}^2} \frac{|\widehat{\psi^*}(\vec{k}, w)|^2}{|\vec{k}|^2|w|}, \, d^2\vec{k}dw < +\infty. \quad (32)$$

The 2D+t continuous wavelet transform of the image sequence $f \in \mathcal{H}$ and wavelet $\Omega_\Lambda\psi$, is scalar product of f and $\Omega_\Lambda\psi$, considered as a function of $(a, \vec{b}, \tau, \beta, c)$[13, 14, 23].

$$W_{a,\vec{b},\tau,\beta,c} = \langle\Omega_\Lambda\psi|f\rangle \quad (33)$$
$$= \int_{\mathbb{R}}\int_{\mathbb{R}^2} \Omega_\Lambda\psi(\vec{x}, t)f(\vec{x}, t)\, d\vec{x}dt \quad (34)$$
$$= \int_{\mathbb{R}}\int_{\mathbb{R}^2} \psi_{a,\beta,c}(\vec{x} - \vec{b}, t - \tau)f(\vec{x}, t)\, d\vec{x}dt, \quad (35)$$

where

$$\psi_{a,\beta,c}(\vec{x}, t) = a^{-3/2}\psi\big(\frac{c^{-p}}{a}r_\beta^{-1}(\vec{x}), \frac{c^q}{a}t\big), \quad (36)$$

or, equivalently in the space of Fourier transforms,

$$\widehat{\psi}_{a,\beta,c}(\vec{k}, w) = a^{3/2}\widehat{\psi}\big(ac^p r_\beta^{-1}(\vec{k}), ac^{-q}w\big). \quad (37)$$

The condition 32 is called the wavelet admissibility condition. To guarantee that this integral is finite, we must ensure that

$$\widehat{\psi}(\vec{0}, w) = 0 \quad \forall w \in \mathbb{R}, \quad (38)$$

$$\widehat{\psi}(\vec{k}, 0) = 0 \quad \forall\vec{k} \in \mathbb{R}^2, \quad (39)$$

which explains why wavelets must have a zero average. This condition is nearly sufficient. If 38 and 39 are satisfies and $\widehat{\psi}$ is continuously differentiable, then the admissibility condition is satisfied.

4. MULTISELECTIVITY SPATIO-TEMPORAL ANALYSIS

In this section we propose a multiselectivity spatio-temporal analysis, defined by Isotropic wavelet, and Anisotropic wavelets with different angular selectivity. The angular selectivity of these wavelets growths with selectivity level. We first construct a isotropic wavelet in spatial frequency variables

$$\widehat{\psi}(\vec{k}, w) = \widehat{\phi}(r)\widehat{\varphi}(w), \qquad r = \|\vec{k}\|, \quad (40)$$

where $\widehat{\phi}$ and $\widehat{\varphi}$ are Fourier transforms of two 1D-wavelets and satisfies the following properties

$$\widehat{\phi}(0) = \widehat{\varphi}(0) = 0. \quad (41)$$

The application of spatio-temporal dilation, rotation, and speed tuning to wavelet ψ gives:

$$\widehat{\psi}_{a,c}(\vec{k}, w) = a^{3/2}\widehat{\phi}(ac^p r)\widehat{\varphi}(ac^{-q}w). \quad (42)$$

The wavelet $\widehat{\psi}$ is shown in Figure 1, and in Figure 2, we show the isotropic wavelet $\widehat{\psi}_{a,c}$ together with speed-tunings at $c > 1$, $c = 1$, $c < 1$ speeds and scale $a = 2$.
When the aim is to detect directional velocity , one has to use a spatial directional wavelets[24, 20, 25].

DEFINITION 1. *A 2D wavelet ψ is said to be directional if the effective support of its Fourier transform $\widehat{\psi}$ is contained in a convex cone in frequency space, with apex at the origin.*

A directional wavelet ψ is characterized by its angular selectivity (or Angular Resolving Power), that is, its ability to distinguish features with close orientations. This quantity is by definition inversely proportional to the aperture of the support cone of $\widehat{\psi}$.

We consider 2π-periodic function d_α defined by

$$d_\alpha(\theta) = \begin{cases} \gamma(\frac{\theta-\alpha}{\alpha}), & \theta \in [0, 2\alpha]; \\ 1, & \theta \in [2\alpha, \pi]; \\ \gamma(\frac{\pi+\alpha-\theta}{\alpha}), & \theta \in [\pi, \pi + 2\alpha]; \\ 0, & \theta \in [\pi + 2\alpha, 2\pi]. \end{cases} \quad (43)$$

where $\alpha \in [0, \pi]$ and the function γ is defined in $[-1, 1]$ and satisfies the following property :

$$\gamma^2(t) + \gamma^2(-t) = 1. \quad (44)$$

For $L \in \mathbb{N}^*$ and $\alpha = \frac{\pi}{2^L}$, we create 2^l different 2π-periodic functions $\eta_{l,m}$ indexed by $0 \le m < 2^l$ for any $l \in \{0, ..., L\}$ and defined by:

$$\eta_{0,0}(\theta) = 1, \quad (45)$$

$$\eta_{l+1,2m}(\theta) = \eta_{l,m}(\theta)d_\alpha(\theta - \frac{(2m+1)\pi}{2^l}), \quad (46)$$

$$\eta_{l+1,2m+1}(\theta) = \eta_{l,m}(\theta)d_\alpha(\theta - \frac{(2m+1)\pi}{2^l} - \pi). \quad (47)$$

We construct a new wavelet whose Fourier transforms are:

$$\widehat{\psi}_{a,m,c,l}(\vec{k}, w) = \widehat{\psi}_{a,c}(\vec{k}, w)\, \eta_{l,m}(\theta), \quad (48)$$

where
$r = \|\vec{k}\|$, and $\theta = \arg\vec{k}$.

PROPOSITION 1. *for any $l \in \{1, ..., L\}$*

$$\eta_{l,0}(\theta) = \begin{cases} \gamma(\frac{\theta-\alpha}{\alpha}), & \theta \in [0, 2\alpha]; \\ 1, & \theta \in [2\alpha, \frac{\pi}{2^{l-1}}]; \\ \gamma(\frac{\frac{\pi}{2^{l-1}}+\alpha-\theta}{\alpha}), & \theta \in [\frac{\pi}{2^{l-1}}, \frac{\pi}{2^{l-1}} + 2\alpha]; \\ 0, & \theta \in [\frac{\pi}{2^{l-1}} + 2\alpha, 2\pi]. \end{cases} \quad (49)$$

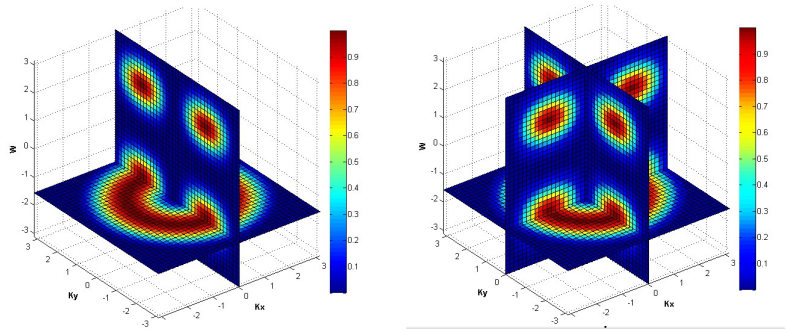

Fig. 1. 3D sectional views of isotropic wavelet $\widehat{\psi}$ in Fourier space (k_x, k_y, w).

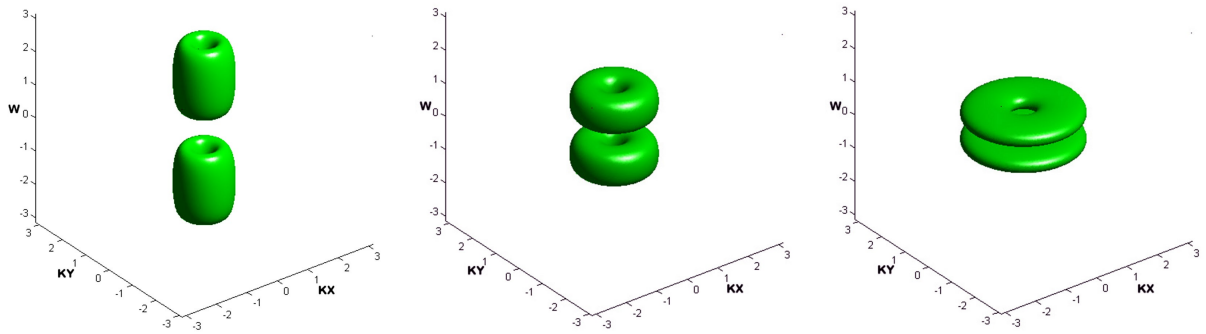

$c < 1$ $c = 1$ $c > 1$

Fig. 2. The 2D+T isotropic wavelet $\psi_{a,c}$ tuned to various velocities with 3D view.

and $\forall m \in \{0, ..., 2^l - 1\}$

$$\widehat{\psi}_{a,m,c,l}(\vec{k}, w) = \widehat{\psi}_{a,c}(r, w)\eta_{l,0}(\theta - \beta_{l,m}), \tag{50}$$

where

$$\beta_{l,m} = m\frac{2\pi}{2^l}. \tag{51}$$

PROOF. According to the expression (43) of the function d_α, one have for any $l \in \{1, ..., L\}$:

$$d_\alpha(\theta - \frac{\pi}{2^l}) = \begin{cases} 0, & \theta \in [0, \frac{\pi}{2^l}]; \\ \gamma(\frac{\theta - \frac{\pi}{2^l} - \alpha}{\alpha}), & \theta \in [\frac{\pi}{2^l}, \frac{\pi}{2^l} + 2\alpha]; \\ 1, & \theta \in [\frac{\pi}{2^l} + 2\alpha, \frac{\pi}{2^l} + \pi]; \\ \gamma(\frac{\pi + \frac{\pi}{2^l} + \alpha - \theta}{\alpha}), & \theta \in [\frac{\pi}{2^l} + \pi, \frac{\pi}{2^l} + \pi + 2\alpha]; \\ 0, & \theta \in [\frac{\pi}{2^l} + \pi + 2\alpha, 2\pi], \end{cases} \tag{52}$$

$$d_\alpha(\theta - \pi - \frac{\pi}{2^l}) = \begin{cases} 1, & \theta \in [0, \frac{\pi}{2^l}]; \\ \gamma(\frac{\frac{\pi}{2^l} + \alpha - \theta}{\alpha}), & \theta \in [\frac{\pi}{2^l}, \frac{\pi}{2^l} + 2\alpha]; \\ 0, & \theta \in [\frac{\pi}{2^l} + 2\alpha, \frac{\pi}{2^l} + \pi]; \\ \gamma(\frac{\theta - \pi - \frac{\pi}{2^l} - \alpha}{\alpha}), & \theta \in [\frac{\pi}{2^l} + \pi, \frac{\pi}{2^l} + \pi + 2\alpha]; \\ 1, & \theta \in [\frac{\pi}{2^l} + \pi + 2\alpha, 2\pi]. \end{cases} \tag{53}$$

We shall now prove that for any $l \in \{1, ..., L\}$

$$\eta_{l,0}(\theta) = \begin{cases} \gamma(\frac{\theta - \alpha}{\alpha}), & \theta \in [0, 2\alpha]; \\ 1, & \theta \in [2\alpha, \frac{\pi}{2^{l-1}}]; \\ \gamma(\frac{\frac{\pi}{2^{l-1}} + \alpha - \theta}{\alpha}), & \theta \in [\frac{\pi}{2^{l-1}}, \frac{\pi}{2^{l-1}} + 2\alpha]; \\ 0, & \theta \in [\frac{\pi}{2^{l-1}} + 2\alpha, 2\pi]. \end{cases} \tag{54}$$

Let's prove this by induction: Since $\eta_{1,0}(\theta) = \eta_{0,0}(\theta)d_\alpha(\theta - \pi - \pi) = d_\alpha(\theta)$, the function $\eta_{1,0}$ expressed as (54). Now assume that for a fixed l, the function $\eta_{l,0}$ expressed as (54). The inclusion of this induction hypothesis and equation (53) in the expression (46) gives:

$$\eta_{l+1,0}(\theta) = \begin{cases} \gamma(\frac{\theta - \alpha}{\alpha}), & \theta \in [0, 2\alpha]; \\ 1, & \theta \in [2\alpha, \frac{\pi}{2^l}]; \\ \gamma(\frac{\frac{\pi}{2^l} + \alpha - \theta}{\alpha}), & \theta \in [\frac{\pi}{2^l}, \frac{\pi}{2^l} + 2\alpha]; \\ 0, & \theta \in [\frac{\pi}{2^l} + 2\alpha, 2\pi]. \end{cases} \tag{55}$$

This last result completes the proof of the induction.
The insertion of the expressions (52) and (54) in equation (47) shows that: for any $l \in \{1, ..., L\}$

$$\eta_{l,1}(\theta) = \begin{cases} 0, & \theta \in [0, \frac{\pi}{2^{l-1}}]; \\ \gamma(\frac{\theta - \frac{\pi}{2^{l-1}} - \alpha}{\alpha}), & \theta \in [\frac{\pi}{2^{l-1}}, \frac{\pi}{2^{l-1}} + 2\alpha]; \\ 1, & \theta \in [\frac{\pi}{2^{l-1}} + 2\alpha, \frac{\pi}{2^{l-2}}]; \\ \gamma(\frac{\frac{\pi}{2^{l-2}} + \alpha - \theta}{\alpha}), & \theta \in [\frac{\pi}{2^{l-2}}, \frac{\pi}{2^{l-2}} + 2\alpha]; \\ 0, & \theta \in [\frac{\pi}{2^{l-2}} + 2\alpha, 2\pi]. \end{cases} \tag{56}$$

Therefore, for any $l \in \{1, ..., L\}$

$$\eta_{l,1}(\theta) = \eta_{l,0}(\theta - \frac{\pi}{2^{l-1}}). \tag{57}$$

We shall now prove that, for any $l \in \{1, ..., L\}$

$$\eta_{l,m}(\theta) = \eta_{l,0}(\theta - \beta_{l,m}) \qquad m = 0, 1, ..., 2^l - 1. \tag{58}$$

with $\beta_{l,m} = m\frac{2\pi}{2^l}$.
Let's prove this by induction: Now assume that for a fixed l:

$$\eta_{l,m}(\theta) = \eta_{l,0}(\theta - \beta_{l,m}), \qquad m = 0, 1, ..., 2^l - 1, \tag{59}$$

The inclusion of the induction hypothesis and equation (57) in the expressions (46) and (47) gives:

$$\begin{aligned}\eta_{l+1,2m}(\theta) &= \eta_{l,m}(\theta)\tau_\alpha(\theta-\pi-\frac{(2m+1)\pi}{2^l})\\ &= \eta_{l,0}(\theta-\beta_{l,m})\tau_\alpha(\theta-\pi-\beta_{l,m}-\frac{\pi}{2^l})\\ &= \eta_{l,0}(\theta-\beta_{l+1,2m})\tau_\alpha(\theta-\pi-\beta_{l+1,2m}-\frac{\pi}{2^l})\\ &= \eta_{l+1,0}(\theta-\beta_{l+1,2m}),\end{aligned}$$

$$\begin{aligned}\eta_{l+1,2m+1}(\theta) &= \eta_{l,m}(\theta)\tau_\alpha(\theta-\frac{(2m+1)\pi}{2^l})\\ &= \eta_{l,0}(\theta-\beta_{l,m})\tau_\alpha(\theta-\beta_{l,m}-\frac{\pi}{2^l})\\ &= \eta_{l,0}(\theta-\beta_{l+1,2m})\tau_\alpha(\theta-\beta_{l+1,2m}-\frac{\pi}{2^l})\\ &= \eta_{l+1,1}(\theta-\beta_{l+1,2m})\\ &= \eta_{l+1,0}(\theta-\beta_{l+1,2m+1}).\end{aligned}$$

□

The proposition shows that for any $l \in \{1,...,L\}$ the parameter m describes a rotation of angle $\beta_{l,n} = n\frac{2\pi}{2^l}$:

$$\begin{aligned}\widehat{\psi}_{a,m,c,l}(\vec{k},w) &= \widehat{\psi}_{a,c}(r,w)\eta_{l,m}(\theta) &(60)\\ &= \widehat{\psi}_{a,c}(r,w)\eta_{l,0}(\theta-\beta_{l,m}) &(61)\\ &= \widehat{\psi}_{a,0,c,l}(r^{-1}_{\beta_{l,m}}\vec{k},w) &(62)\\ &= \widehat{\psi}_{a,c}(r,w)\eta_{l,m}(\theta) &(63)\\ &= \widehat{\phi}(ac^p r)\eta_{l,0}(\theta-\beta_{l,m})\widehat{\varphi}(ac^{-q}w) &(64)\\ &= \widehat{\psi}_l(ac^p r^{-1}_{\beta_{l,m}}\vec{k},c^{-q}w), &(65)\end{aligned}$$

with

$$\widehat{\psi}_l(\vec{k},w) = \widehat{\phi}(r)\eta_{l,0}(\theta)\widehat{\varphi}(w). \quad (66)$$

for each level of construction l, the functions $\eta_{l,m}$ are continuous with compact support of size $\frac{2\pi}{2^l}+2\alpha$. So the aperture of the cone supporting of $\widehat{\psi}_{a,m,c,l}$ is equal to $\frac{2\pi}{2^l}+2\alpha$, the 3D frequency view and the support properties of these wavelets are illustrated in figures 3 and 4 . Indeed, the parameter l determines a selectivity level and the angular selectivity of these wavelets grow with l. In particular, $\widehat{\psi}_{a,0,c,0} = \widehat{\psi}_{a,c}$ is a totally isotropic wavelet.

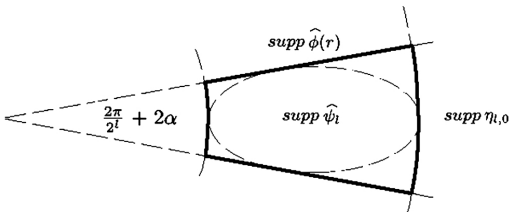

Fig. 4. Support properties of the directional wavelet $\widehat{\psi}_l$.

If the Fourier transform of wavelet ψ_l is continuously differentiable, admissibility condition is satisfied

$$c_\psi = 2\pi^3\int_{\mathbb{R}^2}\int_{\mathbb{R}}\frac{|\widehat{\psi}^*(\vec{k},w)|^2}{|\vec{k}|^2|w|},\ dw\,d^2\vec{k} < +\infty. \quad (67)$$

The 2D+t continuous wavelet transform of the video sequence f and wavelet $\Omega_\Lambda\psi_l(\vec{x},t) = T^{\vec{b},\tau}R^{\beta_{l,m}}A^cD^a\psi(\vec{x},t)$, is scalar product of f and $\Omega_\Lambda\psi_l(\vec{x},t)$

$$\begin{aligned}W_{a,\vec{b},\tau,\beta_{l,m},c,l} &= \langle\Omega_\Lambda\psi_l|f\rangle &(68)\\ &= \int_{\mathbb{R}}\int_{\mathbb{R}^2}\Omega_\Lambda\psi_l(\vec{x},t)f(\vec{x},t)\,d\vec{x}dt. &(69)\end{aligned}$$

Alternatively, the 2D+t continuous wavelet transform can be expressed in wavenumber-frequency domain $(\vec{k},w)$

$$\begin{aligned}&W_{a,\vec{b},\tau,\beta_{l,m},c,l} &(70)\\ &= \widehat{\langle\Omega_\Lambda\psi_l|\widehat{f}\rangle} &(71)\\ &= \int_{\mathbb{R}^2}\int_{\mathbb{R}}e^{-j(\vec{k}.\vec{b}-w\tau)}\widehat{\psi}_{a,m,c,l}(\vec{k},w)f(\vec{k},w)\,d\vec{k}dw &(72)\\ &= \int_{\mathbb{R}}\int_{S_1}\int_{\mathbb{R}_+}\widehat{\psi}_{a,c}(r,w)\eta_{l,m}(\theta)J(r,\theta,w)rdrd\theta dw, &(73)\end{aligned}$$

with

$$J(r,\theta,w,\widetilde{r},\sigma,\tau) = \widehat{f}(r,\theta,w)e^{-j\,(r\widetilde{r}\cos(\sigma-\theta)+w\tau)}, \quad (74)$$

$\widetilde{r} = \|\vec{b}\|$ and $\sigma = \arg\vec{b}$. The last equation may be rewritten as

$$W(a,\vec{b},\tau,\beta_{l,m},c,l) = \langle\eta_{l,n}/R_{a,\vec{b},c}\rangle_{S_1}, \quad (75)$$

where $\langle f/g\rangle_{S_1} = \int_{S_1}f^*(\alpha)g(\alpha)\,d\alpha$, is the scalar product on the circle S_1 of the 2π-periodic functions f and g, and

$$R_{a,\vec{b},c}(\theta) = \int_{\mathbb{R}}\int_{\mathbb{R}^+}\widehat{\psi}_{a,c}(r,w)\,\widehat{f}(r,\theta,w).J(r,\theta,w,\widetilde{r},\sigma,\tau)\,rdr\,dw \quad (76)$$

In other words, the relation 75 means that the wavelet coefficients of the image f can be interpreted as the angular approximation at angular selectivity 2^l of $R_{a,\vec{b},c}$, on a kind of scaling function $\eta_{l,n}$ localized in $\theta_n \in S_1$.
The multiselectivity spatio-temporal analysis of the of image sequence f can be defined as the set of wavelet coefficients up to a selectivity level L, over the spatial and temporal variables $\vec{b}\in\mathbb{R}^2$ and $\tau\in\mathbb{R}$, while fixing the velocity parameters $c\in\mathbb{R}^+$ and the scale $a\in\mathbb{R}^+$.

$$[W_{a,\vec{b},\tau,\beta_{l,m},c,l}, \vec{b}\in\mathbb{R}^2, \tau\in\mathbb{R}, 0\le n<2^l, 0\le l\le L]. \quad (77)$$

5. FREQUENCY-DOMAIN IMPLEMENTATION

In this section we show how to construct examples of wavelets ψ_l, for $l\in\{0,1,...,L\}$, satisfying the properties described in sections 3 and 4. The 2D+T continuous wavelet transform of image sequence f and wavelet $\Omega_\Lambda\psi$, is convolution product of f and $\psi_{a,\theta,c}$ in $(\vec{b},\tau)\in\mathbb{R}^2\times\mathbb{R}$

$$\begin{aligned}&W_{a,\vec{b},\tau,\beta_{l,m},c,l} &(78)\\ &= \langle\Omega_\Lambda\psi_l|f\rangle &(79)\\ &= \int_{\mathbb{R}}\int_{\mathbb{R}^2}\Omega_\Lambda\psi_l(\vec{x},t)f(\vec{x},t)\,d\vec{x}dt &(80)\\ &f(\vec{x},t)\,dtd^2\vec{x} &(81)\\ &= [a^{3/2}\psi(\frac{c^{-p}}{a}r^{-1}_{\beta_{l,m}}.,\frac{c^q}{a}.)*f(.,.)](\vec{b},\tau) &(82)\\ &= [\psi_{a,\beta_{l,m},c,l}*f](\vec{b},\tau). &(83)\end{aligned}$$

The values $W_{a,\vec{b},\tau,\beta_{l,m},c,l}$ are represented as the result of inverse Fourier transform of the product $\widehat{\psi}_{a,\beta_{l,m},c,l}$ and $\widehat{f}$,

$$\widehat{W}_{a,\beta_{l,m},c,l}(\vec{k},w) = \widehat{\psi}_{a,\beta_{l,m},c,l}(\vec{k},w)\widehat{f}(\vec{k},w). \quad (84)$$

Therefore, if f and ψ is band-limited, that is, if $f,\psi\in\mathcal{B}_\pi$

$$\mathcal{B}_\pi = \{h\in\mathcal{H} : \widehat{h}(\vec{k},w) = 0\ if\ \ (\vec{k},w)\notin[-\pi,\pi)^3\}, \quad (85)$$

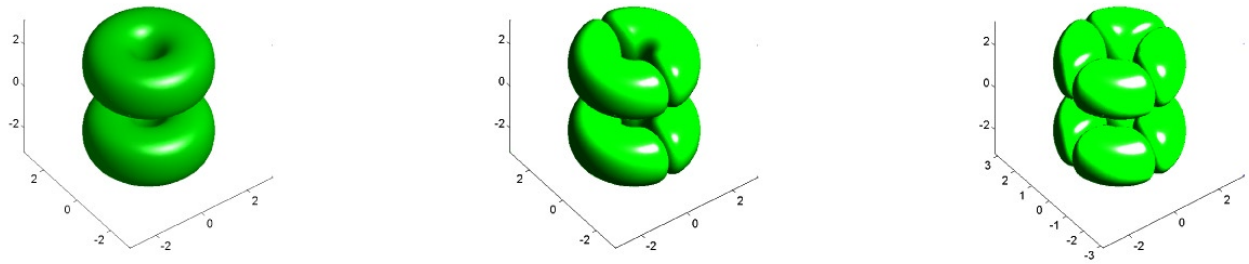

a b c

Fig. 3. The 3D view of 2D+T wavelets $\widehat{\psi}_{2,m,1,l}$: (**a**) $l = 1$ and $m = 0$. (**c**) $l = 1$ and $m \in \{0, 1\}$. (**b**) $l = 2$ and $m \in \{0, 1, 2, 3\}$.

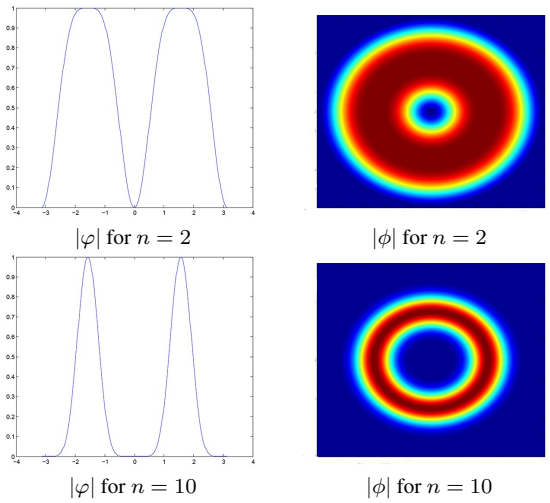

$|\varphi|$ for $n = 2$ $|\phi|$ for $n = 2$

$|\varphi|$ for $n = 10$ $|\phi|$ for $n = 10$

Fig. 5. The spatial spline wavelet$\widehat{\phi}$ and temporal spline wavelet $\widehat{\varphi}$.

the fast Fourier transform (FFT3D) implementation permits to compute $W_{a,\vec{b},\tau,\beta_{l,m},c,l}$. In this particular context, we construct the isotropic wavelet described in section 4.
The spline 1D-wavelet is a good candidate for it owns the properties of compactness in time and frequency, as seen before, which offers the possibility to realize computations in the Fourier space while keeping a good accuracy in the temporal speed domain [21].

$$\widehat{\phi}(r) = \sqrt{2}\exp(\frac{-i\varepsilon r}{1})sin(r/\sqrt{2})^n \sum_{s=0}^{n} cos(r/\sqrt{2})^{2s}, \quad (86)$$

$$\widehat{\varphi}(w) = \sqrt{2}\exp(\frac{-i\varepsilon r}{1})sin(w/\sqrt{2})^n \sum_{s=0}^{n} cos(w/\sqrt{2})^{2s}, \quad (87)$$

with $\varepsilon = 0$ for n even and $\varepsilon = 1$ for n odd. The spatial and temporal selectivity of $\widehat{\varphi}$ and $\widehat{\phi}$ is an important point in this approach, in figure 5, we show that this selectivity is controlled by the parameter n. It's clear that the Fourier transform of wavelets ϕ and φ are continuously differentiables and

$$\widehat{\phi}(0) = 0, \quad (88)$$

$$\widehat{\varphi}(0) = 0, \quad (89)$$

then the admissibility condition is satisfied

$$c_\psi = 2\pi^3 \int_{\mathbb{R}^2}\int_{\mathbb{R}} \frac{|\widehat{\psi}^*(\vec{k},w)|^2}{|\vec{k}|^2|w|}, \, dw\, d^2\vec{k} \quad (90)$$

$$= 4\pi^4 \int_{\mathbb{R}+} \frac{|\widehat{\phi}(r)|^2}{r} dr \int_{-\pi}^{\pi} \frac{|\widehat{\varphi}(w)|^2}{|w|} dw < +\infty. \quad (91)$$

The 2D+t continuous wavelet transform of the image sequence f and wavelet $\Omega_\Lambda\psi_l(\vec{x},t) = T^{\vec{b},\tau}R^{\beta_{l,m}}A^cD^a\psi_l(\vec{x},t)$, is scalar product of f and $\Omega_\Lambda\psi_l(\vec{x},t)$

$$W_{a,\vec{b},\tau,\beta_{l,m},c,l} = \langle\Omega_\Lambda\psi_l|f\rangle \quad (92)$$

$$= \int_{\mathbb{R}^2}\int_{\mathbb{R}} \Omega_\Lambda\psi_l(\vec{x},t)f(\vec{x},t)\, dtd\vec{x}, \quad (93)$$

and

$$\widehat{W}_{a,\beta_{l,m},c,l}(\vec{k},w) = \widehat{\psi}_{a,\beta_{l,m},c,l}(\vec{k},w)\widehat{f}(\vec{k},w), \quad (94)$$

with

$$\widehat{\psi}_{l,0}(\vec{k},w) = \widehat{\psi}(\vec{k},w)\eta_{l,0}(\theta) = \widehat{\phi}(r)\widehat{\varphi}(w)\eta_{l,0}(\theta), \quad (95)$$

$$\widehat{\psi}_{a,\beta_{l,m},c,l}(\vec{k},w) = a^{3/2}\widehat{\phi}(ac^pr)\widehat{\varphi}(ac^{-q}w)\eta_{l,m}(\theta), \quad (96)$$

where $\vec{k} = (r,\theta)$, $r = \|\vec{k}\|$ and $\theta = \arg\vec{k}$.
the properties 46 and 47 imply that for any $l \in \{0, ..., L\}$:

$$\widehat{W}_{a,\check{\beta},c,l+1}(\vec{k},w) \quad (97)$$

$$= \widehat{\psi}_{a,c,0}(r,w)\eta_{l+1,0}(\theta-\check{\beta})\widehat{f}(\vec{k},w) \quad (98)$$

$$= \widehat{\psi}_{a,c,0}(r,w)\eta_{l,0}(\theta-\beta_{l,m})d_\alpha(\theta-\bar{\beta})\widehat{f}(\vec{k},w) \quad (99)$$

$$= \widehat{W}_{a,\beta_{l,m},c,l}(\vec{k},w)d_\alpha(\theta-\bar{\beta}), \quad (100)$$

$$\widehat{W}_{a,\bar{\beta},c,l+1}(\vec{k},w) \quad (101)$$

$$= \widehat{\psi}_{a,c,0}(r,w)\eta_{l+1,0}(\theta-\bar{\beta})\widehat{f}(\vec{k},w) \quad (102)$$

$$= \widehat{\psi}_{a,c,0}(r,w)\eta\eta_{l,0}(\theta-\beta_{l,m})d_\alpha(\theta-\bar{\beta}-\pi)\widehat{f}(\vec{k},w) \quad (103)$$

$$= \widehat{W}_{a,\beta_{l,m},c,l}(\vec{k},w)d_\alpha(\theta-\bar{\beta}-\pi), \quad (104)$$

where $\check{\beta} = \beta_{l+1,2m}$ and $\bar{\beta} = \beta_{l+1,2m+1}$.

6. VELOCITY CAPTURE ALGORITHM

In sections 4 and 5 we constructed a spatio-temporal dictionary

$$\mathcal{D} = [W_{a,\vec{b},\tau,\beta_{l,m},c^j,l}, \vec{b} \in \mathbb{R}^2, \tau \in \mathbb{R}], \quad (105)$$

where $-J \le j \le J$, $0 \le m < 2^l$, and $0 \le l \le L$, this dictionary include more than $(2J+1)(2^{L+1}-1)$ Spatio-Temporal

representations with different angular selectivity l, Orientation $\beta_{l,m}$, and speed c^j. In this section we study the select of the best representation in dictionary $\mathcal{D}$ for tracking motion and velocity capture in image sequence.
We define speed energy density normalized function, which represents the contribution to the signal energy at a given location $(\vec{b},\tau)$, scale a, speed c, orientation $\beta_{l,m}$ and selectivity level l.

$$P_{a,\beta_{l,m},c,l}(\vec{b},\tau) = Nor(|W_{a,\vec{b},\tau,\beta_{l,m},c,l}|^2), \tag{106}$$

where for image sequence $M(\vec{b},\tau)$

$$Nor(M) = \frac{|M| - V_{min}}{V_{max} - V_{min}}, \tag{107}$$

$$V_{min} = \min_{\vec{b},\tau} |M(\vec{b},\tau)|, \tag{108}$$

$$V_{max} = \max_{\vec{b},\tau} |M(\vec{b},\tau)|, \tag{109}$$

The energy density $P_{a,\beta_{l,m},c,L}$ is computed for each selectivity level l over each orientation $\beta_{l,m}$. we define the speed-orientation energy density at selectivity level l as

$$P_{a,c,l}(\vec{b},\tau) = \max_{\beta_{l,m}} P_{a,\beta_{l,m},c,l}(\vec{b},\tau). \tag{110}$$

We can also define the speed-multiselectivity energy density by

$$P_{a,c}(a,\vec{b},\tau) = \max_{l} P_{a,c,l}(\vec{b},\tau). \tag{111}$$

The steps of the proposed velocity capture algorithm are described briefly as follows:

(1) Fix the scale a, the speed c, the largest speed level $J \in \mathbb{N}$ and the highest selectivity level $L \in \mathbb{N}$.
(2) Calculate $\widehat{f}$ by 3D FFT.
(3) Calculate the Fourier transform of isotropic wavelets $\widehat{\psi}_{a,c^j,0}$,

$$\widehat{\psi}_{a,c^j,0}(\vec{k},w) = a^{3/2}\widehat{\phi}(ac^{jp}r)\widehat{\varphi}(ac^{-jq}w) \quad -J \le j \le J. \tag{112}$$

(4) Multispeed tuning in the Fourier space $\widehat{W}_{a,c^j,0}(\vec{k},w)$ computed by the convolution the image sequence and wavelets in Fourier space:

$$\widehat{W}_{a,c^j,0}(\vec{k},w) = \widehat{\psi}_{a,c^j,0}(\vec{k},w)\widehat{f}(\vec{k},w). \tag{113}$$

(5) Multiselectivity decomposition in the Fourier space $[\{\widehat{W}_{a,\beta_{l,m},c^j,l}\}_{-J\le j\le J,0\le m<2^l,0\le l\le L}]$ computed from $\widehat{W}\widehat{\psi}_{a,c^j,0}(\vec{k},w)$ by equations 97 and 101.
(6) Apply 3D inverse FFT to get the multiselectivity spatio-temporal analysis $[W_{a,\vec{b},\tau,\beta_{l,m},c^j,l}, J \le j \le J, 0 \le m < 2^l, 0 \le l \le L]$.
(7) Compute energy densities $P_{a,\beta_{l,m},c^j,l}$,$P_{a,c^j,l}$ and P_{a,c^j}.

7. APPLICATIONS

As a first application, we tested our velocity capture algorithm at a sequence of four rectangles in isotropic motion and vertical translations at two constant speeds in the plane: two rectangles are in vertical translation with speeds $v_1 = 0.5$ and $v_2 = 2$ pix/fr and two are in rotation motion with the same speeds. We refer to this sequence as the test 1 sequence, and it contains 130 frames of 240x240 pixels. A spatio-temporal representation of trajectories of rectangles in this sequence are shown in figure 6. In the experiments, we choose $a = 2$, $c = \sqrt{2}$, $J = 4$ and $L = 4$.

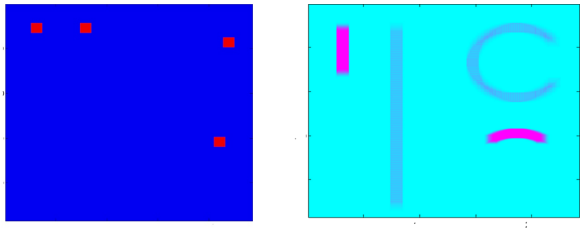

a b

Fig. 6. (a) First frame of test 1 sequence. (b) Motion trajectories of the four rectangles.

The figure 7 shows isotropic wavelet energy density $P_{a,c^j,0}$ for frames 20 and 60 with different speeds. The two speeds corresponding to the isotropic motion are clearly identified from isotropic wavelets and coincide with the velocities present in the tiest1 sequence (The maximums are exactly reached for $c^{-2} = 0.5 = v_1$ pixels/fr and $c^2 = 2 = v_2$ pixels/fr), but for the directional motion, the poor angular selectivity of wavelet, thus makes the directional capture of the vertical translation very difficult. This does not happen with high selectivity level $L = 4$ and vertical orientation, as shown in figures 8 and 9.

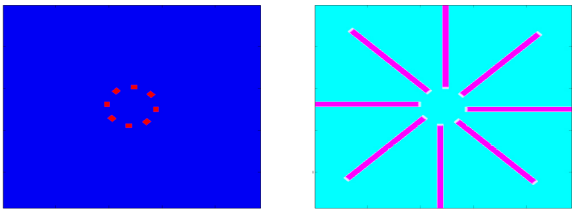

a b

Fig. 10. (a) First frame of test 2 sequence. (b) Motion trajectories of the four rectangles.

We also tested our velocity capture algorithm using a sequence of four rectangles in different directional translations with speed $v_1 = 1$ pix/fr . We refer to this sequence as the test 2 sequence and contains 130 frames of 240x240 pixels. A spatio-temporal representation of trajectories of rectangles in this sequence are shown in figure 10. In figure 11, We show that speed-multiselectivity energy density P_{a,c^0} can represent the signal directional speed at all orientation.
.

8. CONCLUSION

We have introduced a new algorithm for Motion and speed analysis in video sequences, based on the concept of angular multiselectivity. In this paper, we have developed in frequency domain a new spatio-temporal wavelets with variable angular selectivity, the 2D+T continuous wavelet transform of these new wavelets can generate a multiselectivity analysis, wich can capture the different structures of the motion and velocity, and we have succeeded in demonstrating that our 2D+T wavelets are very effective for the calculation of motion parameters.

9. REFERENCES

[1] C. Zhu, W.S. Qi, and W. Se. Predictive fine granularity successive elimination for fast optimal block-matching motion estimation. *IEEE Transactions on Image Processing*, 10(2):213221, 2005.
[2] T. Koga, K. Iinuma, A. Hirano, Y. Iijima, and T. Ishiguro. Motion compensated inter-frame coding for video conferencing. *Proceedings of the NTC81*, pp. C.9.6.19.6.5,, 1981.

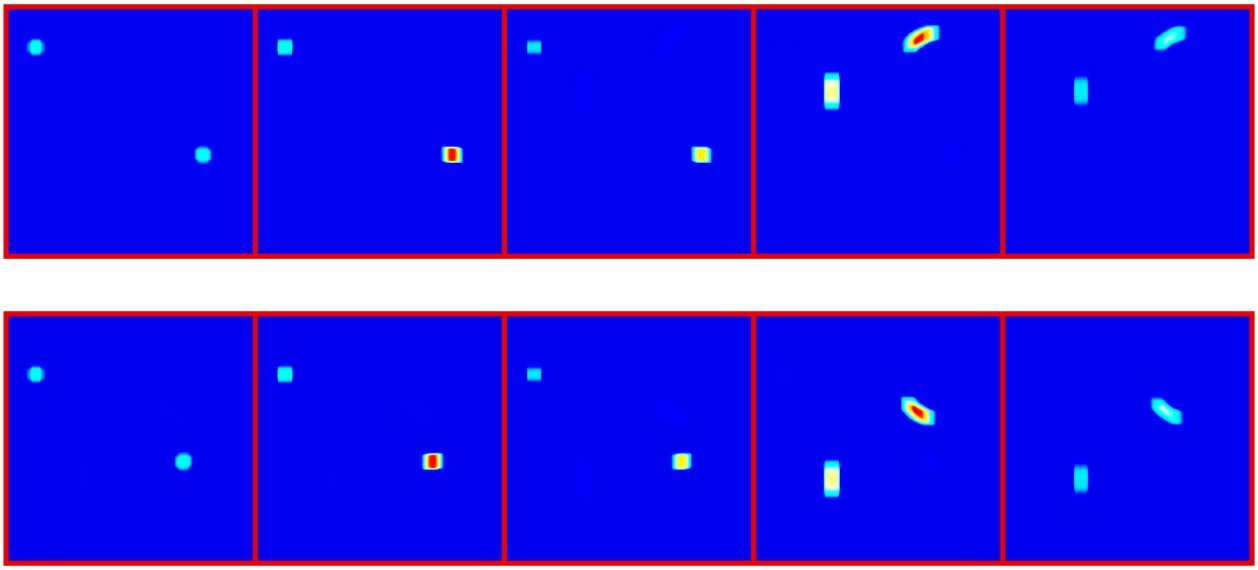

$j = -4$ $j = -2$ $j = 0$ $j = 2$ $j = 4$

Fig. 7. This figure shows a isotropic speed analysis and motion detection via speed energy density $P_{2,c^j,0}$ for frames 20 and 60 of test 1 sequence.

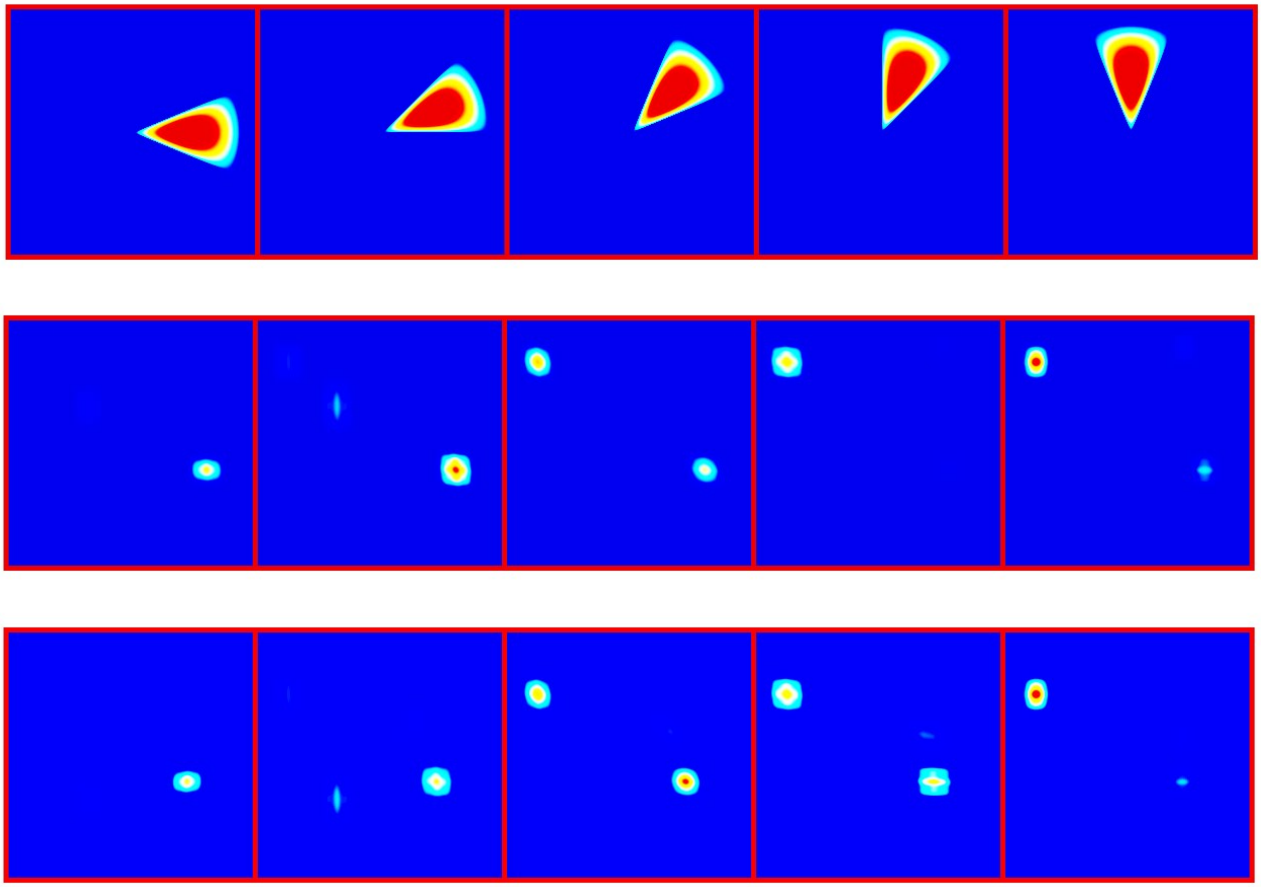

$\beta_{4,0}$ $\beta_{4,1}$ $\beta_{4,2}$ $\beta_{4,3}$ $\beta_{4,4}$

Fig. 8. Directional speed detection ($c^{-2} = 0.5$ pixels/fr) via energy densities $P_{2,\beta_{4,m},c^{-2},4}$ for frames 20 and 60 of test 1 sequence.

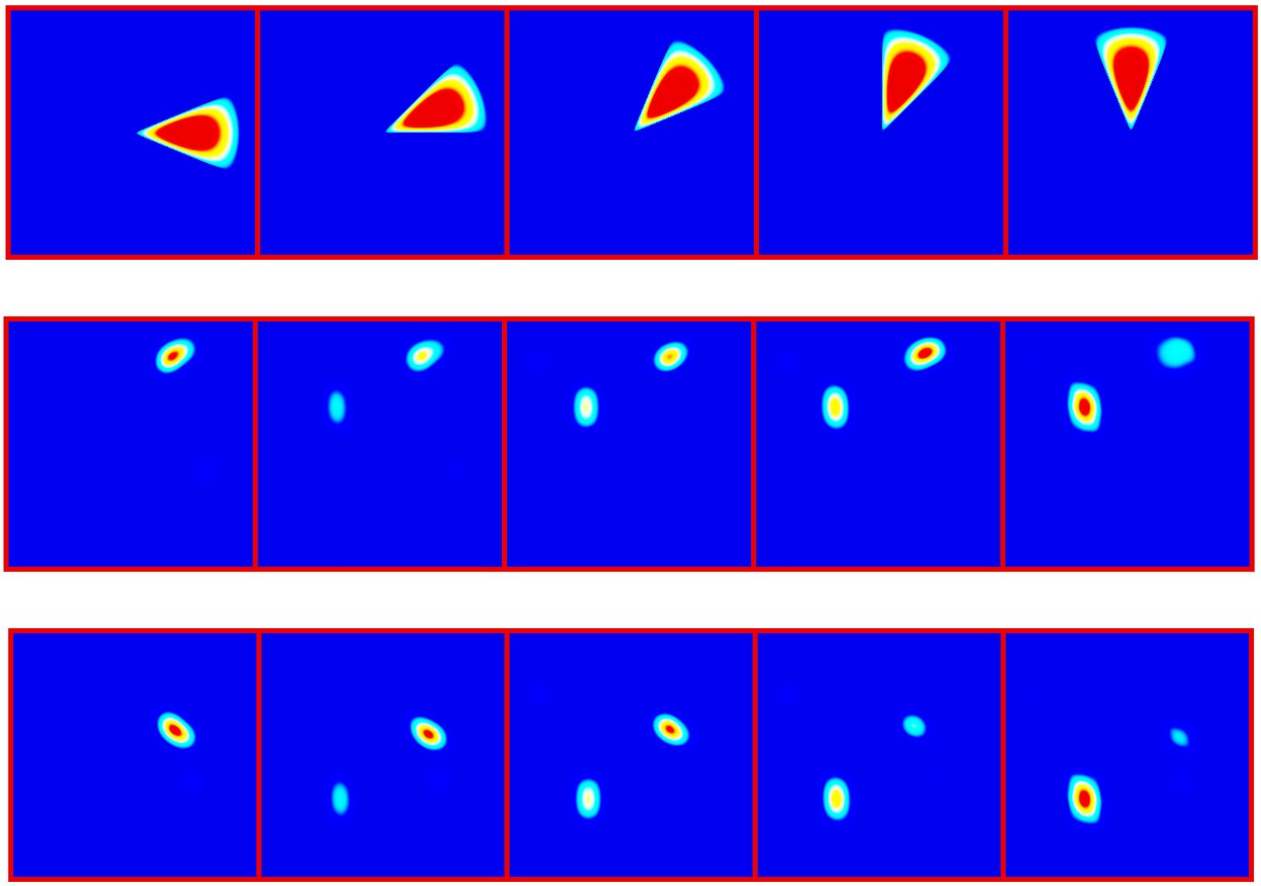

$\beta_{4,0}$ $\beta_{4,1}$ $\beta_{4,2}$ $\beta_{4,3}$ $\beta_{4,4}$

Fig. 9. Directional speed detection ($c^2 = 2$ pixels/fr) via energy densities $P_{a,\beta_{4,m},c^2,4}$ for frames 20 and 60 of test 1 sequence.

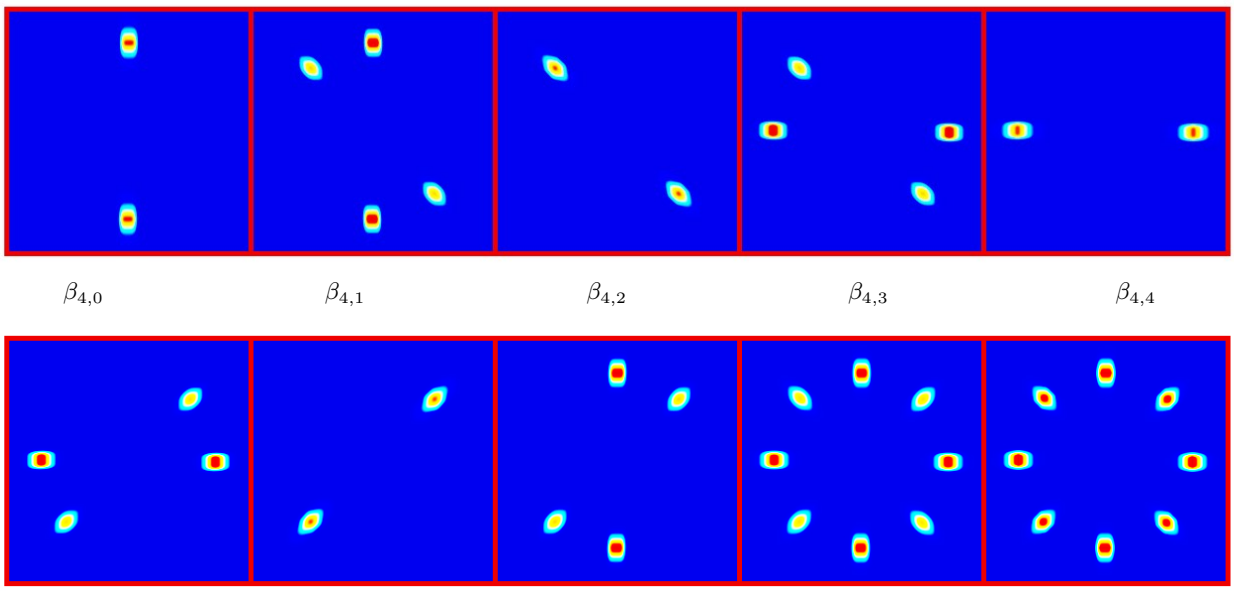

$\beta_{4,0}$ $\beta_{4,1}$ $\beta_{4,2}$ $\beta_{4,3}$ $\beta_{4,4}$

$\beta_{4,5}$ $\beta_{4,6}$ $\beta_{4,7}$ $P_{2,c^0,4}$ P_{2,c^0}

Fig. 11. Multiselectivity speed detection ($c^0 = 1$pixels/fr) via energy densities $P_{2,\beta_{4,m},c^0,4}$, $P_{2,c^0,4}$ and P_{2,c^0} for frame 20 of test2 sequence.

[3] A. Ess, K. Schindler, B. Leibe, and L. Van Goo. Object detection and tracking for autonomous navigation in dynamic environments. *The International Journal of Robotics Research*, 29(14):1707–1725.

[4] M. Betke, E. Haritaoglu, and LS. Davis. Real-time multiple vehicle tracking from a moving vehicle. *Mach Vision Appl*, 12(2):69–83, 2000.

[5] A. Taboada-Crispi, H. Sahli, and M.O. Monteagudo. Anomaly detection in medical image analysis. *Handbook of Research on Advanced Techniques in Diagnostic Imaging and Biomedical Applications*, Publisher: IGI Global(2009).

[6] Y. Wang, K.F Loe, T. Tan, and J-K. Wu. Spatiotemporal video segmentation based on graphical models. *IEEE transactions on image processing*, 14:937–947, July 2005.

[7] W. Brendel and S. Todorovic. Video object segmentation by tracking regions. *IEEE 12th International Conference on Computer Vision*, pages 833–840, 2009.

[8] M. El Aallaoui and A. Gourch. Video segmentation using 2d+time mumford-shah functional. *International Journal of Computer Applications (0975 - 8887)*, 55(3):15–22, 2012.

[9] Z. Wang, X. Gao, B. Zhang, and H. Wu. Motion estimation for a mobile robot based on real-time stereo vision system. *2nd International Congress on Image and Signal Processing*, pages 1–5, 2009.

[10] J.J Tsai and H. Ming Hang. Modeling of pattern-based block motion estimation and its application. *IEEE Transactions on Circuits and Systems for Video Technology*, 19(1):108–113.

[11] C. Zhu, W. S. Qi, and W. Ser. Predictive fine granularity successive elimination for fast optimal block-matching motion estimation. *EEE Trans. Image Process*, 14(2):213221, 2005.

[12] C.P. Bernard. Ondelettes et problmes mal poss : la mesure du flot optique et l'interpolation irrgulire. *PhD thesis, Ecole Polytechnique, CMAP, Centre de Mathematiques Appliques.*, 1999.

[13] F. Mujica. Spatio-temporal continuous transform for motion estimation. *hD Thesis*, 1999.

[14] P. Brault. Motion estimation and segmentation. *PhD thesis*, 2005.

[15] M. Duval-Destin. Analyse spatiale et spatio-temporelle de la stimulation visuelle l'aide de la transforme en ondelettes. *Thse de Doctorat*, 1991.

[16] M. Duval-Destin and R. Murenzi. Spatio-temporal wavelets: Application to the analysis of moving patterns. *in Progress in Wavelet Analysis and Applications*, 1992.

[17] P. Brault and J.P Antoine. A spatio-temporal gaussian-conical wavelet with high aperture selectivity for motion and speed analysis. *Applied and Computational Harmonic Analysis*, 34:148–161, 2013.

[18] J-P Antoine. Galilean wavelets: Coherent states of the affine galilei group. *Journal of Mathematical Physics*, 40(11), 1999.

[19] J.-P. Leduc, J. Corbett, M. Kong, V. M. Wickerhauser, and B. K. Ghosh. Accelerated spatio-temporal wavelet transforms: An iterative trajectory estimation. *IEEE ICASSP5*, page 7772780, 1998.

[20] J-P. Antoine, R. Murenzi, P. Vandergheynst, and S.T. Ali. Two-dimensional wavelets and their relatives. *Cambridge University Press*, 2004.

[21] S. Mallat. A wavelet tour of signal processing. *Academic Press*, 1998.

[22] J-P. Antoine, P. Carrette, R. Murenzi, and B. Piette. Image analysis with two-dimensional continuous wavelet transform. *Signal Processing*, 31:241272, 1993.

[23] S. T. Ali, J-P. Antoine, and J-P. Gazeau. Coherent states, wavelets and their generalizations. *Springer*, 2000.

[24] J-P. Antoine and R. Murenzi. Two-dimensional directional wavelets and the scale-angle representation. *Signal Processing*, page 259281, 1996.

[25] M. ElAallaoui, A. ElBouhtouri, and A. Ayadi. Adaptive selectivity representation: Design, and applications. *Int. J. Wavelets, Multiresolution and Information Processing (ijwmip)*, 7:89–113, 2009.